1 Performance Studies based on Inclusive Data

1.1 Reconstruction of kinematic variables

The kinematics of inclusive DIS processes are usually discussed in terms of x and Q^2. Various different methods are available to reconstruct these quantities, using either the scattered electron, the inclusive hadronic final state (defined as all remaining final state particles after excluding the electron) or a mixture of the two. In each of the methods, Q^2 is typically best reconstructed and x is obtained indirectly using $Q^2 = sxy$. The variable y, which is closely related to the scattering angle in the lepton-quark centre-of-mass frame and thus also to the direction of the hadronic final state in the laboratory frame, is therefore a vital ingredient and is often used to quantify and compare the performance of different reconstruction methods.

Figures 1 and 2 summarize the predicted resolutions obtained by ATHENA on the y variable throughout the accessible kinematic plane in x and Q^2 at an example beam energy combination of $18\ \mathrm{GeV}$ electrons in collision with $275\ \mathrm{GeV}$ protons. In common with previous DIS experiments, the electron-only method performs best over most of the kinematic phase space and will be used for neutral current (NC) DIS measurements at all but the lowest y values. The ATHENA ECAL energy measurements and at lower p_T tracker momentum measurements provide an excellent level of performance. At the lowest y values, the electron method resolution degrades like $1/y$. Here, the ability of ATHENA to reconstruct the overall hadronic final state with good resolution can be exploited using the $e - \Sigma$ method, to recover high quality measurements down to $y \sim 10^{-3}$, leading to high quality reconstruction in the crucial high x region.

In charged current (CC) DIS, the only available method is Jacquet-Blondel (JB), which relies entirely on the hadronic final state. Once again, the high quality response of ATHENA to hadrons over a wide range of η and p_T leads to a good level of performance.

The y resolution for different kinematic ranges are shown individually for the scattered electron method, the JB method, the Double-Angle (DA) method, the Sigma method, and the e-Sigma method in figures $3 - 6$. The Q^2 resolution for the various methods is shown in figure 7.

Additional resolution studies for the lowest EIC energy setting $-$ 5 GeV electrons on 41 GeV protons are shown for the y variable in figure 8 and the Q^2 variable in figure 9.

Good reconstruction of the inclusive kinematic quantities requires good acceptance and reconstruction efficiency for both charged and neutral particles. The pseudo-rapidity distributions of the generated (red curves) and reconstructed (blue curves) positive pions, electrons, and photons are shown in figures 10, 11, and 12, respectively. The results are shown for the highest EIC energy setting, for inclusive DIS data in the kinematic range $Q^2 > 10\ GeV^2/c^2$.

1.1.1 Methodology

In order to extract resolutions for the inclusive kinematic variables, the question of reconstruction resolution was factorized from the question of particle identification. The following procedure was used for the reconstruction plots shown above. First, the reconstructed scattered electron was identified based on a comparison of the momenta and angle of the reconstructed tracks with the true scattered electron on the generator level. Next, all additional tracks (charged particles) were matched to generator-level particles to determine the particle species of the track. The reconstruction of the charged particles, therefore, relied on the tracking information combined with the truth-level particle identification information. Any additional tracks not matched to generated-level particles were also included in the reconstruction, with an assumed mass equal to zero.

The charged particles were then associated with energy clusters in the electromagnetic and hadronic calorimeters. These clusters were removed. The remaining clusters were matched to a generator-level neutral particle $-$ and then reconstructed using the cluster energy and angle combined with the truth-level particle identification information. Any addition clusters which were

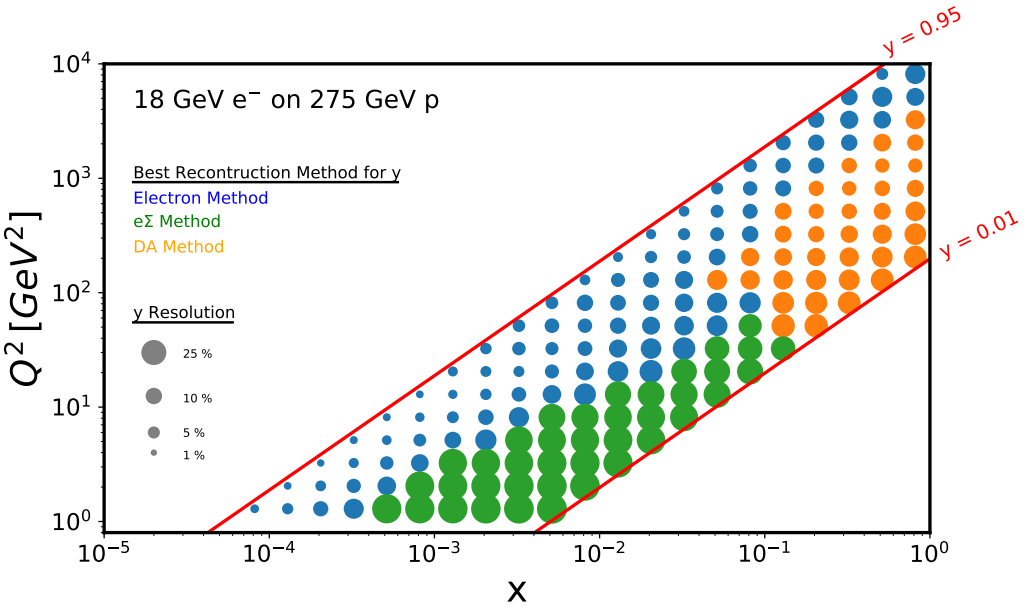

Figure 1: Variation of the estimated ATHENA resolution on the kinematic variable, y, with x and Q^2, for the example case of $18\ \mathrm{GeV}$ electrons colliding with $275\ \mathrm{GeV}$ protons. At each point in the kinematic plane, the best performing reconstruction method is chosen and indicated by the colour of the corresponding marker, while the size of the marker indicates the magnitude of the resolution obtained.

not associated with either a charged particle track or a generator-level neutral particle are also reconstructed, with an assumed mass equal to zero.

For the incoming electron and hadron beams, event by event fluctuations in the momenta are included in simulated data. Since these fluctuations are not know for a given event, the reconstruction is performed using constant beam momenta.

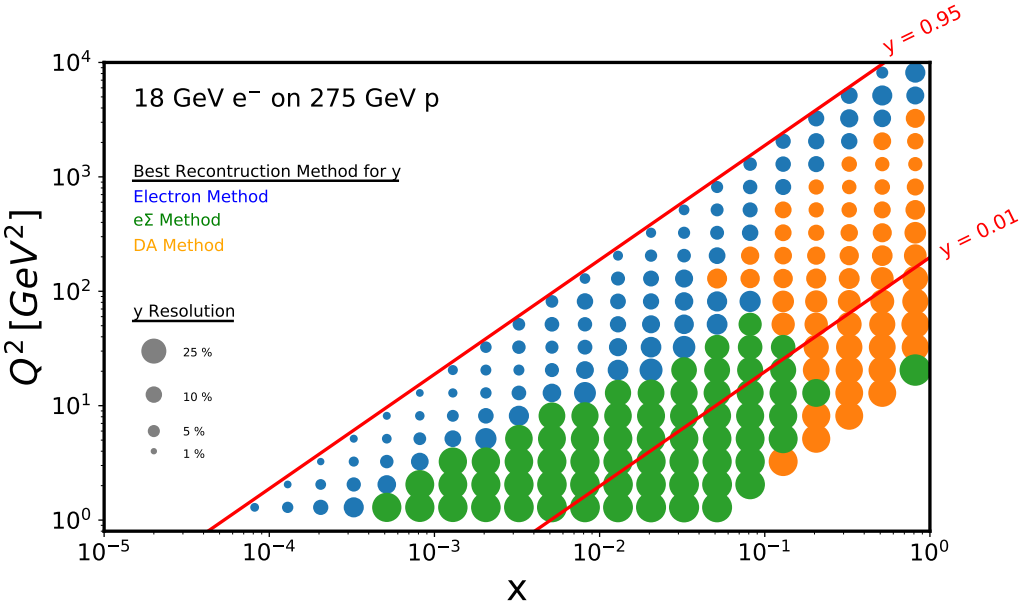

Figure 2: Same as figure 1, except with data extended down to $y = 10^{-3}$.

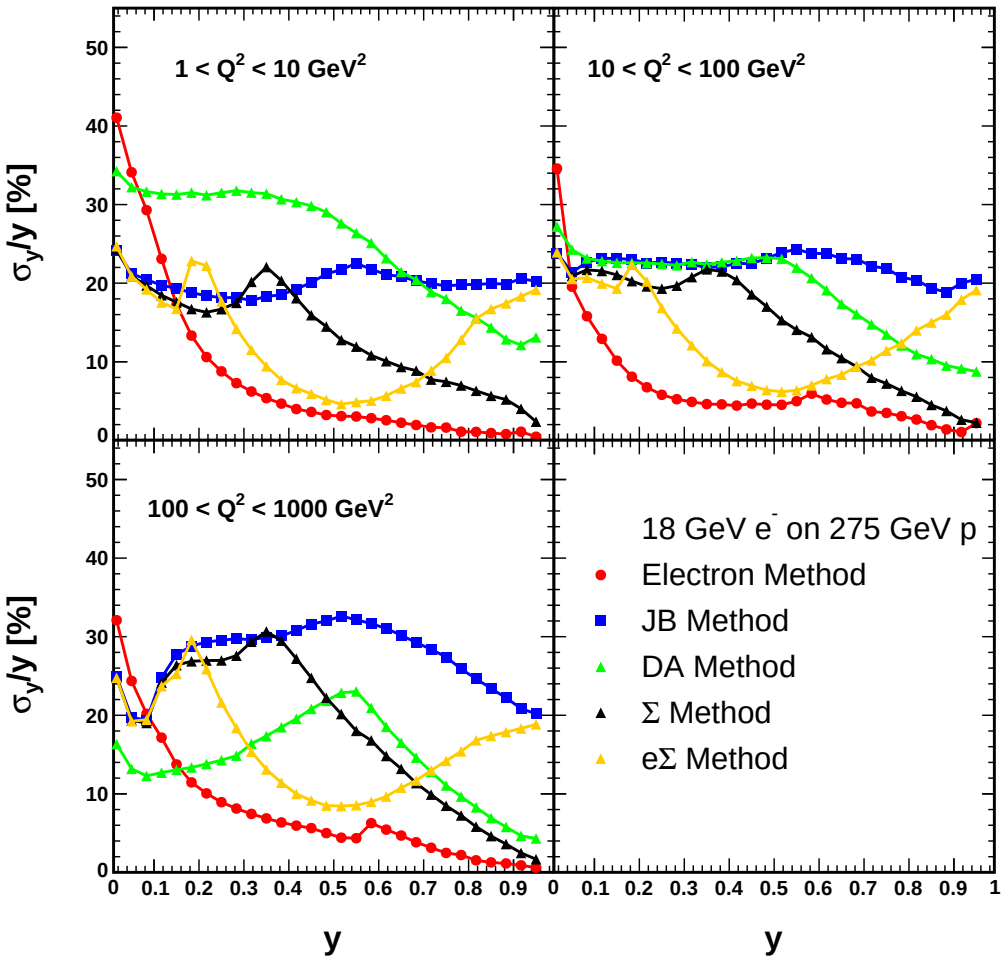

Figure 3: Percent y resolution as a function of y for five different reconstruction methods. The results are shown for various kinematic ranges as shown on the plots. The x-axis is in linear scale.

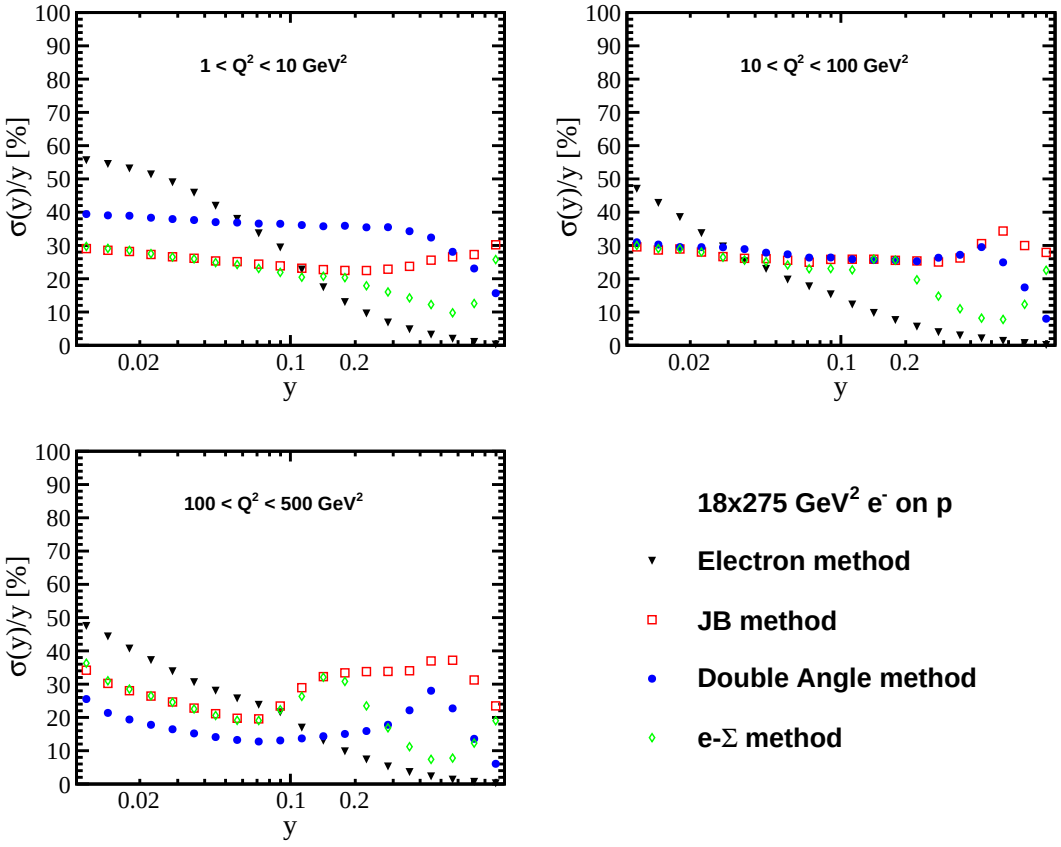

Figure 4: Percent y resolution as a function of y for four different reconstruction methods. The results are shown for various kinematic ranges as shown on the plots. The x-axis is in log scale.

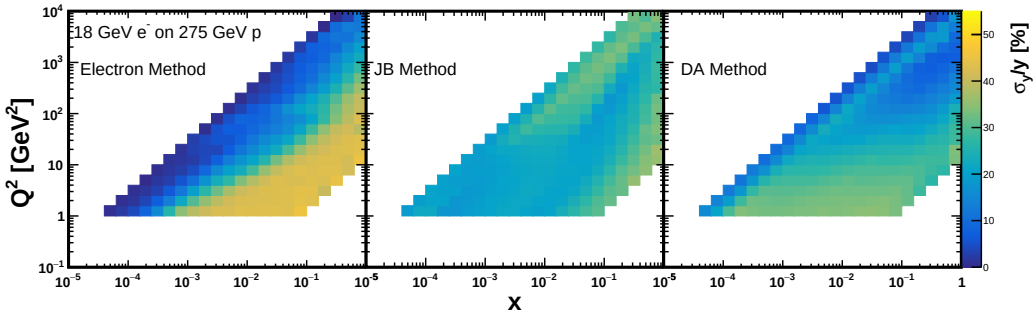

Figure 5: Percent y resolution in the $Q^2 - x$ space for the scattered electron method (left), the Jacquet-Blondel method (center), and the Double-Angle method (right).

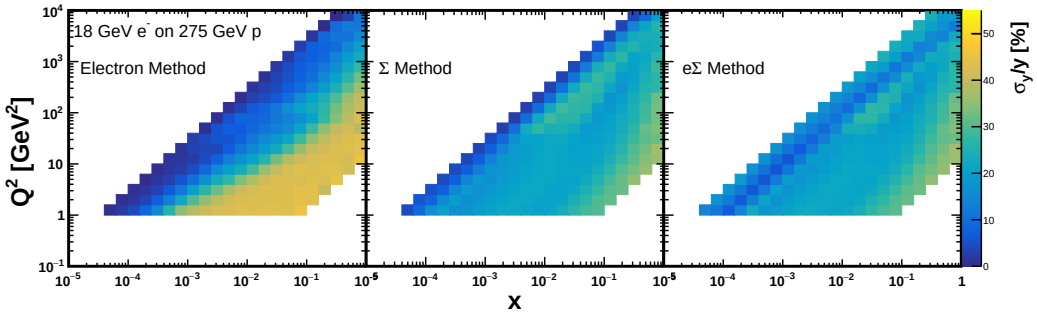

Figure 6: Percent y resolution in the $Q^2 - x$ space for the scattered electron method (left), the Sigma method (center), and the e-Sigma method (right).

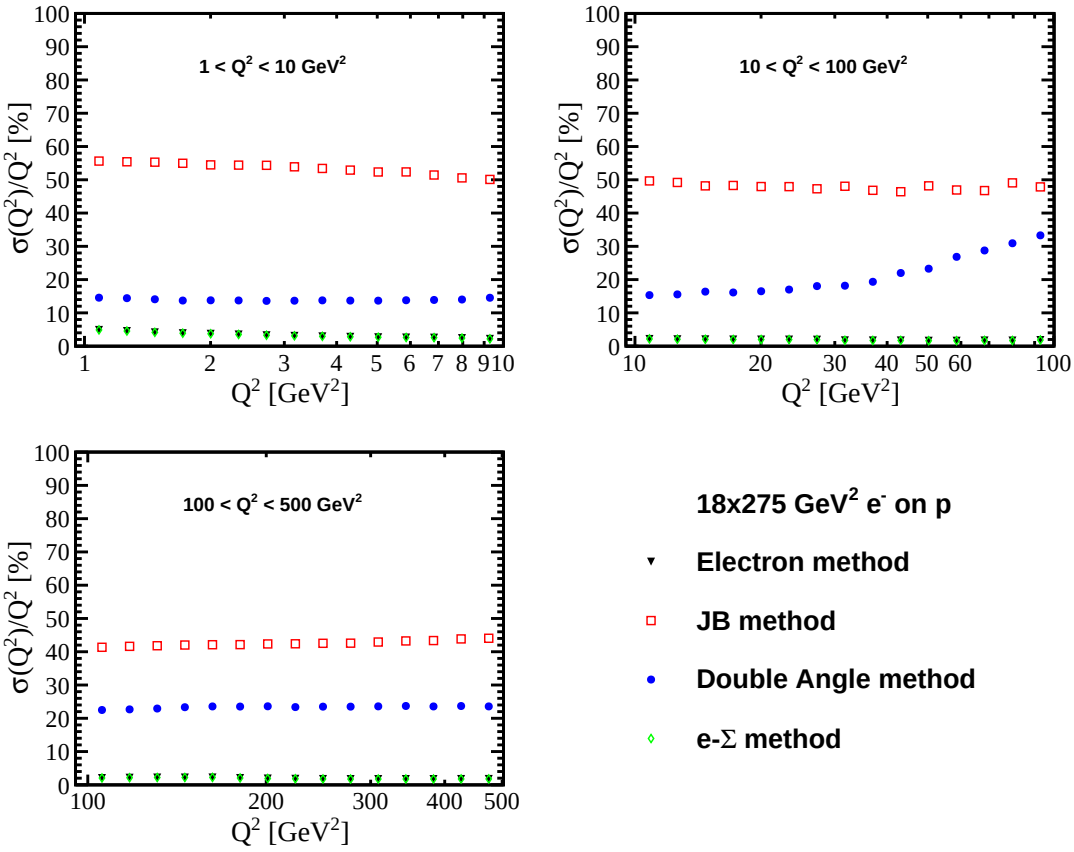

Figure 7: Percent Q^2 resolution as a function of Q^2 for four different reconstruction methods. The results are shown for various kinematic ranges as shown on the plots.

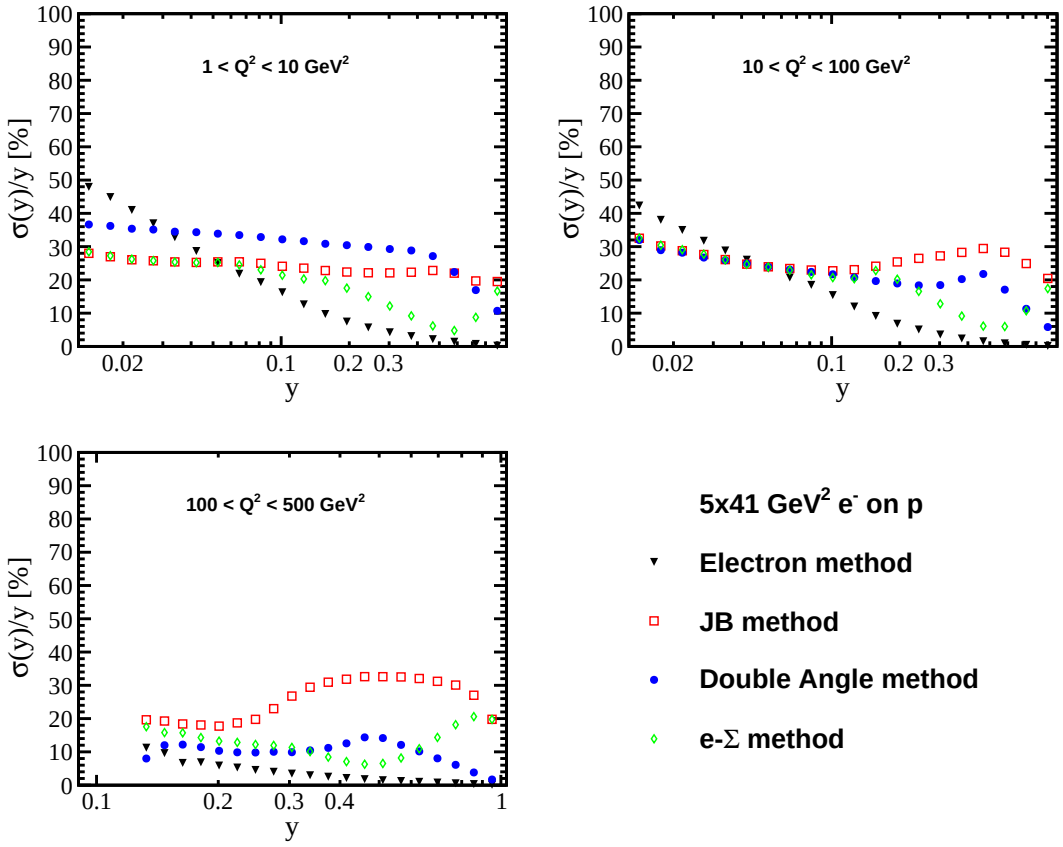

Figure 8: Percent y resolution as a function of y for four different reconstruction methods. The results are shown for various kinematic ranges as shown on the plots, for the lowest beam energy setting – 5 GeV electrons on 41 GeV protons. The x-axis is in log scale.

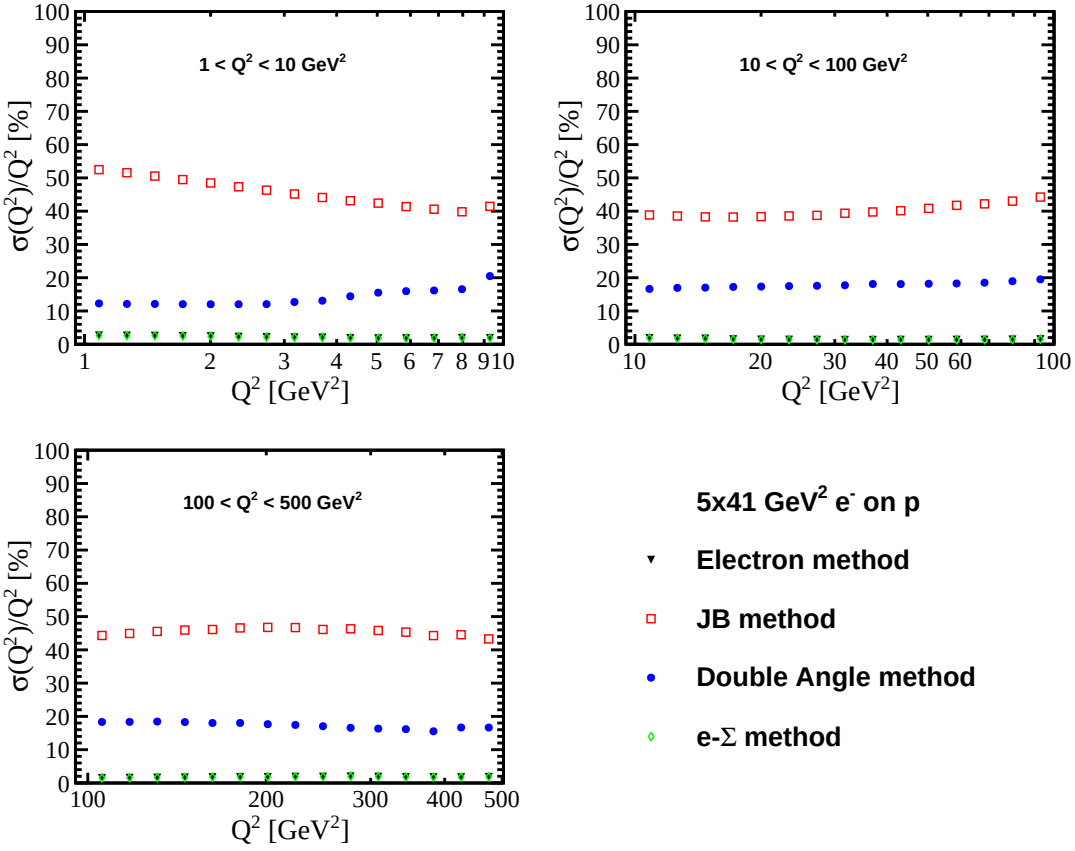

Figure 9: Percent Q^2 resolution as a function of Q^2 for four different reconstruction methods. The results are shown for various kinematic ranges as shown on the plots, for the lowest beam energy setting – 5 GeV electrons on 41 GeV protons.

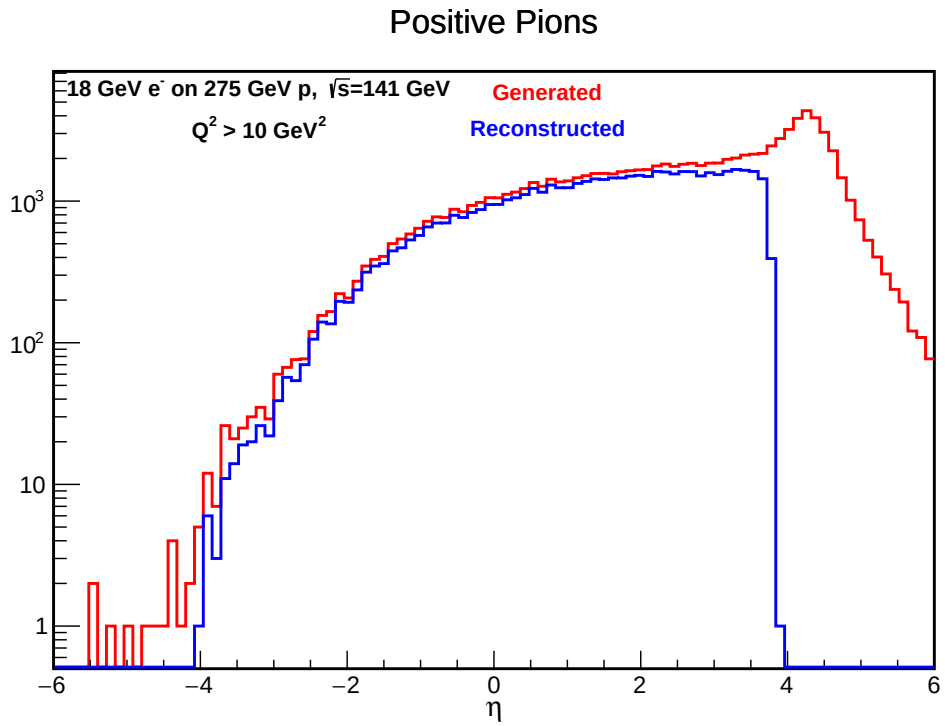

Figure 10: Comparison of the generated and reconstructed pseudo-rapidity distributions for positive pions. The pions are reconstructed using the tracking detector. The distributions are shown for $Q^2 > 10\ GeV^2$.

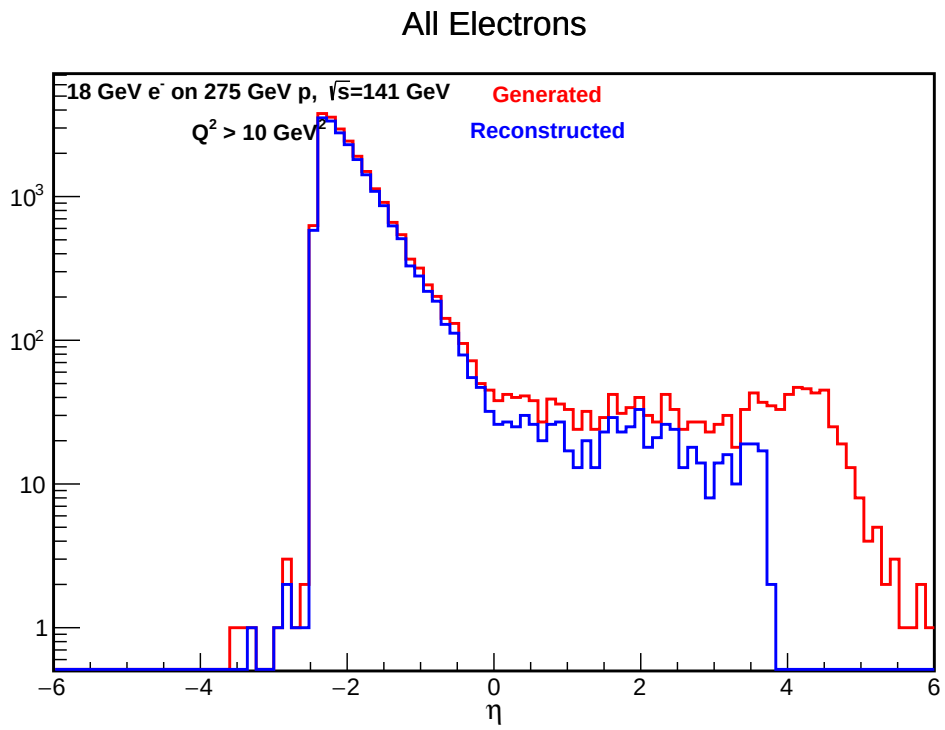

Figure 11: Comparison of the generated and reconstructed pseudo-rapidity distributions for electrons. The electrons are reconstructed using the tracking detector. Both the scattered electron as well as any other electron present in the event are included in the distribution. As can be seen, the yield is highest at lower pseudo-rapidity (which corresponds to the scattered electron at lower Q^2) and then falls rapidly towards higher pseudo-rapidity. For positive values of pseudo-rapidity, the distribution is largely flat, as electrons other than the scattered electron dominate the spectrum. The distributions are shown for $Q^2 > 10\ GeV^2$.

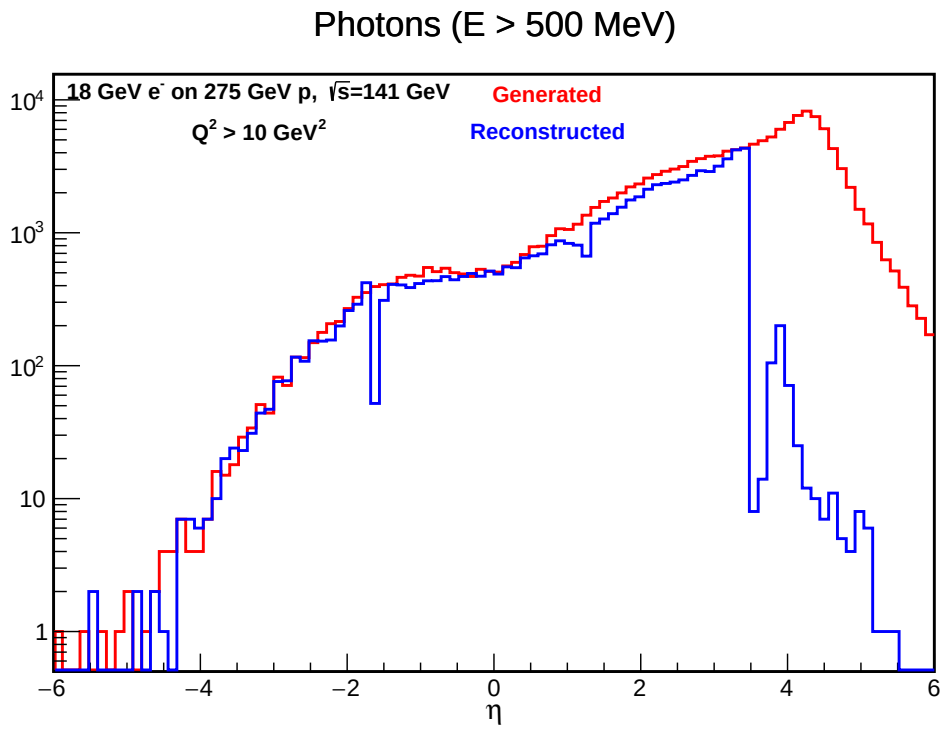

Figure 12: Comparison of the generated and reconstructed pseudo-rapidity distributions for photons. The generated photon is required to have an energy greater than 500 MeV to be included in the red distribution; the reconstructed photon is required to have a detected energy greater than 500 MeV to be included in the blue distribution.

1.2 Background

In addition to the detector acceptance, the kinematic range over which precision measurements can be made in NC DIS also depends on ability to control backgrounds in which the scattered electron signature is faked. This will ultimately be a complicated question involving a variety of sources. However, assuming a selection based on a calorimeter cluster consistent with an electromagnetic object, linked to a track deposited by a charged particle, the dominant background source is expected to arise from residual π^- mesons that pass the calorimeter requirements. The magnitude of this source of background has been estimated as a function of scattered electron energy and pseudorapidity, starting from the e^-/π^- rejection factors obtained in ECAL studies in the backward endcap and barrel regions, which vary strongly with energy between around 10^2 and 10^4 over the relevant range. These factors are convoluted with the predicted yields of electrons and pions in a PYTHIA6 simulation of NC DIS to obtain first estimates of background rates. Some additional background suppression is obtained using the overall event kinematics and topology. An isolation requirement is applied to the scattered electron candidate and it is required that the summed $E-p_z$ of all final state particles within the acceptance range of the main calorimeters ($\eta < 3.5$) be compatible with the expected value of twice the electron beam energy. Together these requirements provide around another factor of 10 suppression of the background.

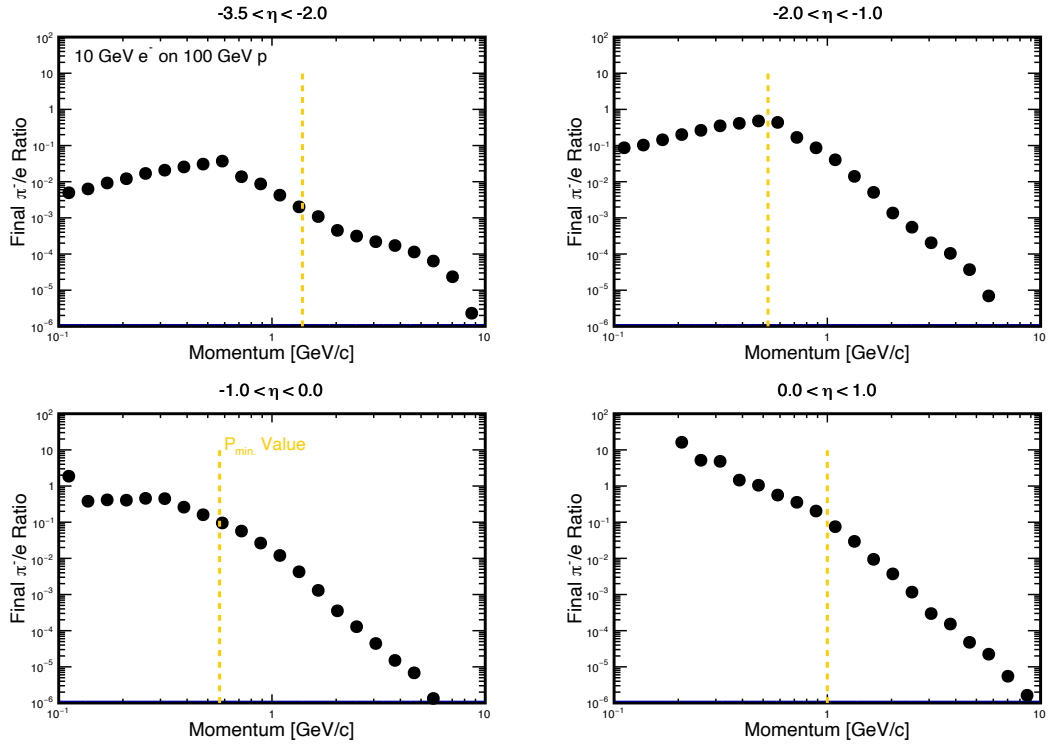

Figure 13: Estimated background fractions to the NC DIS scattered electron selection from π^- mesons as a function of momentum and pseudorapidity for collisions between 10 GeV electrons and 100 GeV protons. The pions are rejected using the basic PID performance of the detector in combination with event-level requirements on the total $E - p_z$ and the electron isolation. The vertical lines indicate the minimum momenta allowed by the requirements $Q^2 > 1$ GeV^2 (important in the most backward η range) and $y < 0.95$ (important in all remaining η ranges).

The results of the π^- background studies are shown in figure 13 for the example of 10 GeV electron and 100 GeV proton beams, as a function of scattered electron momentum for four different ranges in η. The background fractions are generally largest at low momenta. The $1/Q^4$ factor in the cross section implies that the signal electron distribution is strongly peaked towards the back-

ward direction, whereas the pion spectrum is relatively flat in η, such that the background fractions are largest for the most central (highest Q^2) electrons. However, the minimum scattered electron momenta that are allowed by a typical kinematic requirement ($y < 0.95$, see below) also grow with Q^2, such that the estimated π^- background contamination is at or below the 10% level throughout the accessible kinematic range. Maintaining this high level of performance into the large y region is important due to its kinematic correlation with low x.

1.3 Acceptance and Simulated Data

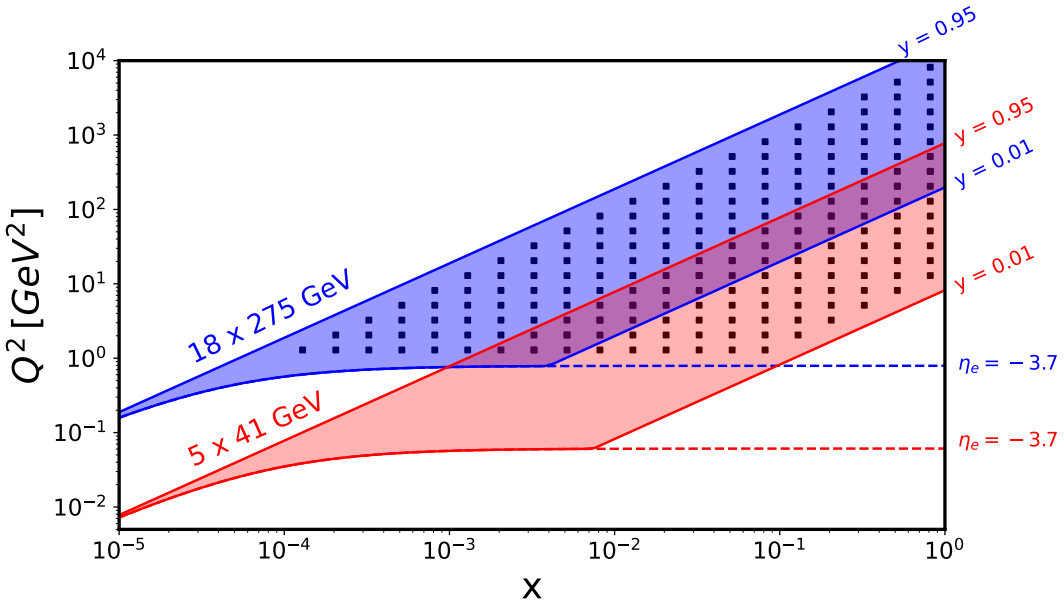

Figure 14: Kinematic coverage and binning of simulated ATHENA data in the deep-inelastic region with the maximum and minimum expected centre-of-mass-energy configurations. Each point is a simulated measurement, subject to the kinematic cuts described in the text.

In order to investigate the sensitivity to the underlying physics, simulated NC DIS ATHENA data have been produced for the cases of unpolarised ep scattering, ep scattering with polarisation of both beams, and unpolarised eA scattering. Figure 14 shows the simulated data for the unpolarised ep case. The kinematic range is restricted to $Q^2 > 1$ GeV^2 corresponding to the deep inelastic regime and a region in which the ATHENA ECAL and tracking detectors provide full acceptance across the accessible x range. The requirement $y < 0.95$ is applied to ensure sufficiently large scattered electron energies and tolerable background conditions (figure 13) and a further cut $y > 0.01$ is made to ensure that the kinematic variables can be sufficiently well reconstructed (figure 1). The resolution throughout the phase space covered comfortably allows for 5 logarithmically spaced bins per decade in each of x and Q^2. A sample size of $100\ fb^{-1}$ is assumed for the beam energy combination producing the highest instantaneous luminosity, corresponding to a year of ATHENA data taking. The other beam energy combinations are scaled according to the expected instantaneous luminosity such that each simulated sample corresponds to equal EIC running time. The integrated luminosities for the 5 beam energy combinations studied are shown in table 1. With these sample sizes, statistical uncertainties for the case of the inclusive ep cross section are negligible at all but the very highest x and Q^2 values. They do, however, become important for the asymmetry measurements that are sensitive to spin dynamics.

With the $y > 10^{-2}$ requirement, the kinematic coverage of the highest and lowest beam energies overlap, with the intermediate beam energy combinations providing access to further measurements within the phase space. Extending the kinematic range to $y > 10^{-3}$ may be possible

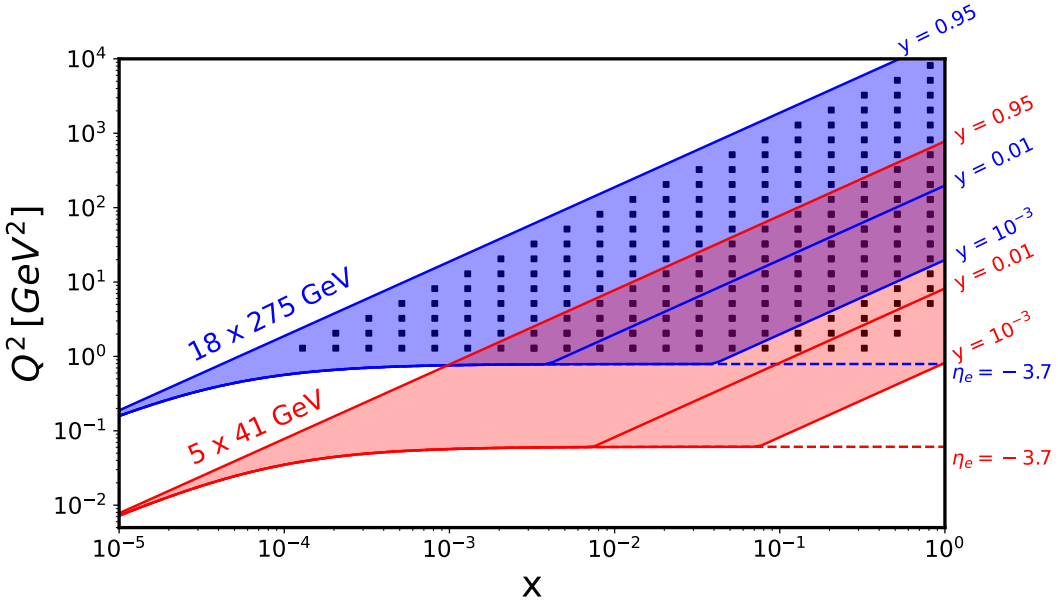

Figure 15: As for 14, but with the y range extended to 10^{-3}. Note that the requirement $W > 2$ GeV becomes relevant for the low Q^2, high x region, leading to the suppression of a handful of data points.

with the use of mixed electron-hadron reconstruction methods (section 1.1). This would result in the kinematic coverage illustrated in figure 15, with an extension to higher x in the low Q^2 region, completing the coverage to photon-proton centre-of-mass energies $W < 2\,\mathrm{GeV}$, where resonances dominate and QCD studies are usually not applied.

Table 1: Summary of ATHENA pseduo-data luminosities at different beam energies

e-beam E	p-beam E	$\sqrt{s}$ (GeV)	inte. Lumi. (fb^{-1})
18	275	140	15.4
10	275	105	100.0
10	100	63	79.0
5	100	45	61.0
5	41	29	4.4

When all beam energy combinations are considered, the ATHENA data cover a wide range of x and Q^2, overlapping with HERA, but with far more extensive coverage and much better precision at large x. This inclusive NC cross section is the fundamental ingredient of all studies of collinear parton densities at EIC, as well as underlying semi-inclusive, exclusive and hadronic final state cross section measurements.

References